

The dwarf galaxy population of the Coma cluster to $M_R = -11$: a detailed description

Neil Trentham

Institute for Astronomy, University of Hawaii
2680 Woodlawn Drive, Honolulu HI 96822, U. S. A.
email : nat@newton.ifa.hawaii.edu

ABSTRACT

We present the luminosity function and measurements of the scalelengths, colours, and radial distribution of dwarf galaxies in the Coma cluster down to $R = 24$. Our survey area is 674 arcmin²; this is the deepest and most detailed survey covering such a large area.

Our measurements agree with those of most previous authors at bright and intermediate magnitudes. The new results are:

- 1) Galaxies in the Coma cluster have a luminosity function $\phi(L) \propto L^\alpha$ that is steep ($\alpha \sim -1.7$) for $-15 < M_R < -11$, and is shallower brighter than this. The curvature in the luminosity function at $M_R \sim -15$ is statistically significant.
- 2) The galaxies that contribute most strongly to the luminosity function at $-14 < M_R < -12$ have colours and scalelengths that are consistent with those of local dwarf spheroidal galaxies placed at the distance of Coma.
- 3) These galaxies with $-14 < M_R < -12$ have a colour distribution that is very strongly peaked at $B - R = 1.3$. This is suggestive of a substantial degree of homogeneity in their star formation histories and metallicities.
- 4) These galaxies with $-14 < M_R < -12$ also appear to be more confined to the cluster core ($r \sim 200$ kpc) than the brighter galaxies. Alternatively, this observation may be explained in part or whole by the presence of an anomalously high number of background galaxies behind the cluster core. Velocity measurements of these galaxies would distinguish between these two possibilities.

Key words: galaxies: clusters: luminosity function – galaxies: clusters: individual: Coma

1 INTRODUCTION

The Coma cluster (Abell 1656) is the prototypical rich cluster of galaxies. It is one of two Abell richness ≥ 2 clusters within 100 Mpc of us, and, of them, is the better studied (the other, Perseus = Abell 426, lies in the Galactic plane). In Table 1, we list its main properties.

The optical morphology of the Coma cluster has been well studied (see, e.g., Rood & Baum 1967). It has two central bright supergiant elliptical galaxies of approximately equal luminosity, NGC 4874 and NGC 4889; this may suggest that Coma is the result of a merger between two smaller subclusters. NGC 4874 has a faint extended halo and has been interpreted as a cD by Schombert (1988). Coma has also been well studied in X-rays (e.g., Briel et al. 1992); it shows considerable substructure – a dominant smooth component centered on NGC 4874 and a smaller component 41 arcminutes to the southwest centered on NGC 4839 (which Schombert also interprets as a cD based on its extended halo). Coma is also notable for the absence of a cooling flow (Hughes et al. 1988); Stewart et al. (1984) suggest that a cooling flow there might have been disrupted if Coma was the result of a merger of two smaller subclusters.

Because the galaxy density is so high, Coma has been a popular place in which to study the galaxy luminosity function (LF), defined as the number density of galaxies per unit luminosity. Early attempts (e.g., Godwin & Peach 1977, Lugger 1986) concentrated on measuring the giant galaxy LF. Since then, we have come to realize that at lower luminosities ($M_B > -17$, or $M_R > -18$), galaxies are almost exclusively members of a separate population of galaxies, the dwarfs (the dwarf spheroidals, or dSphs, sometimes called dwarf ellipticals, and also the dwarf irregulars, or dIrrs). These are a different family of galaxies from giant ellipticals (which are the most numerous kind of giant galaxies in clusters; Dressler 1980) on the fundamental plane parameter correlations (Kormendy 1985, 1987; Binggeli 1994). This suggests that different physical processes are at work in producing their luminosities. Understanding the details of these physical processes has driven much recent theoretical activity. The LF of dwarf galaxies depends mainly on the efficiency with which gas is converted into stars in low mass systems (this efficiency depends on things like the physics of wind ejection). Different models produce extremely different results (compare Figure 14 of Babul & Ferguson 1996 with Figure 2d of White & Kauffmann 1994, for example). Therefore the measurement of the dwarf galaxy LF offers a powerful probe of galaxy formation theories.

The main observational difficulty in measuring the dwarf LF in Coma has been to subtract the background galaxy number counts. This is now a straightforward exercise, because large-format CCDs have permitted us to characterize well the background galaxy number counts and their variance at faint magnitudes (see, e.g., Driver et al. 1994b, Bernstein et al. 1995, Trentham 1997a). The first work on this subject was done by Thompson & Gregory (1993), who determined the LF to $B \sim 20$ ($M_B \sim -15$) with photographic measurements. Their results suggested a steepening of the LF at their faint magnitudes: $\alpha \approx -1.4$. Subsequent measurements quickly followed. Biviano et al. (1995) made velocity measurements of a complete sample of Coma galaxies down to $B = 20$ and found a LF that was rising at the faint-end. Karachentsev et al. (1995) confirmed that there was an excess of faint galaxies above the background and showed that these excess galaxies had systematically lower surface brightnesses than the background galaxies. Bernstein et al. (1995) attempted to measure the Coma LF to much fainter limits ($M_R \sim -9.5$) in a smaller region of the cluster but suffered from globular cluster contamination in the halo of NGC 4874 at faint magnitudes and could not constrain the galaxy LF strongly fainter than $M_R = -14$ in this

region (see their Figure 5). More recently, Secker & Harris (1996, hereafter SH96) made a deep survey over a much larger area (700 arcmin²) and found a LF that is rising to $M_R = -14$ and flattens fainter than this. Their best-fit LF has $\alpha = -1.4$. However, their faintest points depend on a completeness correction; our simulations generally show these corrections to be unreliable (see Trentham 1997a for a discussion of correction methods and their pitfalls) and very sensitive to details like the sizes of the galaxies that are being corrected for. We need deeper imaging of the fields that they studied to get results that are independent of these corrections and to test how valid these worries are. Lobo et al. (1996) argue that $\alpha = -1.81 \pm 0.03$ for $-19 < M_V < -15$; it is unclear why a LF this steep was not seen in the other surveys.

In this work, we extend the measurement of the LF 1.5 magnitudes fainter than SH96 in the R -band. We cover a similar area. We also measure the $B - R$ colours and scalelengths of the faintest dwarfs and investigate how these properties vary with radial position in the cluster. We also attempt to compare them with nearby dwarf galaxies.

The results of Kormendy (1987) suggest that local dSph and dIrr galaxies have exponential light profiles and B -band absolute magnitudes M_B and scalelengths h that are related by the expression

$$M_B = -9.8 \log_{10} h - 16.6,$$

The central surface-brightnesses are

$$\mu_{B0} = M_B + 2.5 \log_{10} 2\pi h^2.$$

In the present work, our measurements are deep enough to detect all galaxies in the Coma cluster obeying this relation with $M_B < -11$ and $M_R < -12$, assuming $B - R > 0.5$ (typically dIrrs have $B - R \approx 1$ and dSphs have $B - R \approx 1.5$; see Trentham 1997b and references therein). The only such galaxies that we do not detect are those that fall within the isophote of a much brighter galaxy (we correct for this). In some of our survey area, we are able to detect galaxies with absolute magnitudes 0.5 mag fainter than the limits above because the image quality is better or because the sky brightness is lower. We use a technique to measure total magnitudes that takes into account the surface brightnesses of the galaxies, which allows us (i) to get realistic estimates of the uncertainties in total magnitudes (ii) to see clearly where completeness worries might be important. This method, along with our observing details, is presented in Section 2. In Section 3 we present and discuss the results.

Throughout this work we assume that $H_0 = 75 \text{ km s}^{-1} \text{ Mpc}^{-1}$.

2 OBSERVATIONS AND PHOTOMETRY

2.1 Data collection and reduction

All observations presented here were taken at the f/10 Cassegrain focus of the University of Hawaii 2.2 m telescope on Mauna Kea during the nights of March 7–9 1994, April 8–10 1994, May 7–8 1994, and May 1–3 1995. The detector was a Tektronix 2048 × 2048 CCD (scale 0".22 pixel⁻¹; field of view 7'.5 × 7'.5). The CCD was thinned and backside-illuminated and it had a high quantum efficiency at short wavelengths, allowing deep imaging. We imaged a total of 654 square arcminutes of the cluster core (see Figure 1) for 35 minutes in B and 25 minutes in R using Mould filters, and a 56 square arcminute region centered on NGC 4839 for 45 minutes in B and R . The imaging of the core region was done as a 4×4 mosaic of individual fields. Each image was constructed from five shorter exposures, dithered

in order to reject bad pixels and to construct sky flats. A substantial dither (30 arcseconds) was needed so that satisfactory median sky flats could be constructed for these fields, which contained several large galaxies. Hence the total survey area is somewhat smaller than the total area of sixteen, $7'.5 \times 7'.5$ frames. The individual exposures were bias-subtracted and then flatfielded using a flatfield that was constructed using both median sky and twilight flats. This produced images flat to better than one percent. The CCD read noise was sufficiently low ($18 e^-$, gain $3.5 e^-/\text{ADU}$) that all the images were dominated by photon noise from the sky. The seeing varied from $0''.7$ to $1''.1$ FWHM.

Instrumental magnitudes were computed from observations of standard stars (~ 30 per night). The photometry was converted to the Johnson (UBV) – Cousins (RI) magnitude system of Landolt (1992). This conversion is accurate to about 2%. Because we need to do an accurate background subtraction to determine the LF, and because the background number counts are a steep function of magnitude, an accurate zero-point is important. We need an uncertainty in the relative zero-point between our cluster and background fields $\Delta m_{\text{zpt}} < 0.035$ mag in R to ensure that the field-to-field variance remains the dominant source of error. Although our zero-point is only 2% accurate relative to an absolute scale, the uncertainty in the relative zero-points between cluster and field will be much less than this (the same standards were used to calibrate both datasets), and the inequality above is easily satisfied.

Conditions were photometric when most of the images were taken; in the few cases when there was thin cirrus overhead, the images were calibrated using shorter exposures taken under photometric conditions.

2.2 Photometry Techniques

2.2.1 Computation of Total Magnitudes and the Luminosity Function

The surface-brightness–dependent technique of making isophotal corrections that we use to measure our galaxy magnitudes is described in detail elsewhere (Trentham 1997a, hereafter T97). A detailed evaluation of the technique as applied to real data is presented there also. The main steps are:

- 1) We measure the rms sky noise σ_{rms} and the seeing FWHM b_{FWHM} for each image.
- 2) We then simulate galaxies of various apparent magnitudes and exponential scalelengths. These simulated galaxies are then convolved with a Gaussian seeing function of width b_{FWHM} , and Poisson noise of rms magnitude σ_{rms} is added. In these simulations we consider all regions of the magnitude–scalelength plane excluding objects that are smaller than point sources and objects that are too big and/or too faint to be detected above the sky noise. Figure 2 of T97 shows a typical such region of this plane.
- 3) We then run the FOCAS detection algorithm (Jarvis & Tyson 1981; Valdes 1982, 1989) to search for objects with fluxes that are $3\sigma_{\text{rms}}$ above the sky. For each object we measure the isophotal magnitude m_I and its first-moment light radius $r_1 = \int r I(\mathbf{r}) d^2\mathbf{r} / \int I(\mathbf{r}) d^2\mathbf{r}$, where \mathbf{r} is the radial vector measured in the plane of the sky from the center of the object and $I(\mathbf{r})$ is the projected light distribution of the object. As the true magnitude m of each object is known in the simulation, we compute the function $m(m_I, r_1)$, and its uncertainty $\sigma(m)[m_I, r_1]$. The uncertainty comes from studying how intrinsically identical galaxies are detected differently depending on the local noise. We also determine the faintest magnitude m_L at which galaxies whose intrinsic magnitudes and scalelengths are equal to those of local dwarf galaxies seen at the distance of Coma are detected with 100% completeness in the absence of brighter galaxies (the magnitude vs. scalelength relation from Section 1 was

used). This will be the faintest magnitude to which we determine the LF in each image. We make this cut because the completeness is a very strong function of magnitude fainter than m_L (it typically drops from 100% to 0% over a range of one magnitude). Therefore completeness corrections would be very unreliable.

4) We then run the same detection algorithm on our data and make a catalog of all objects detected at the 3σ level (typically 26 mag arcsec⁻²) above the sky. For each object, we measure m_I and r_1 .

5) Multiple objects within a single detection isophote are identified by searching for multiple maxima and are split into individual objects using the FOCAS splitting algorithm. The algorithm is run several times, so that cases where many objects were contained in a single isophote initially are all individually recovered. The quantities m_I and r_1 are computed for each object at each stage of the splitting.

6) Objects are then classified based on their morphology relative to that of several reference PSF stars in the field (see Valdes 1989 for the details of the classification terminology).

7) We then remove from the catalog (i) objects with $m(m_I, r_1) < m_L$; (ii) diffraction spikes of bright stars, ghost images, and chip defects (these were identified from the FOCAS classification – see T97 and Valdes 1989 for details); and (iii) objects in the halos of a number of giant elliptical or S0 galaxies having a associated population of red unresolved faint objects that are probably globular clusters. Table 2 lists the relevant galaxies and excluded areas. This is done so that the globular cluster contamination in our faintest one or two bins is small – Bernstein et al. 1995 showed that globular cluster contamination is probably very significant at $R > 24$ in the halo of NGC 4874. We also removed (iv) spurious objects that were detected in the halos of bright stars and galaxies where the noise is much higher than for the rest of the image. The last of these corrections required us to look at all objects in our image that were part of a larger object that was subsequently split into more than three smaller objects in our original detection pass and to make a judgment by eye as to whether the faint objects we see are really galaxies or stars, or local noise peaks that have been enhanced because of the higher sky background in the halo of a bigger galaxy. This was the most time-consuming part of this project, but the effort spent is justified by the increased confidence that all objects that remain in our final catalog are real. Also, at this stage, a number of low-surface-brightness galaxies that had been recognized as a multiple object and split into many small objects centred on local noise peaks were reconstructed, and the values of m_I and r_1 that were computed prior to splitting were adopted.

8) After these corrections are made, we then have a FOCAS catalog of objects classified as “galaxies” or “stars”. At faint magnitudes, these classifications are unreliable because many galaxies have apparent scalelengths smaller than the seeing and so look like stars. We therefore correct for stellar contamination in our images by assuming that the shape of the Galactic stellar luminosity function (SLF) is invariant for $20 < m < 25$, adopting the measured SLF shape of Jones et al. (1991) and computing the number of faint stars as a function of magnitude based on this SLF normalized by the numbers of stars detected at the bright end where the classifications are 100% reliable. For Coma, which lies well out of the Galactic plane, this is a small effect ($< 5\%$), and the uncertainties generated by this method are negligible.

9) From our measured m_I and r_1 values, for each object in our catalog we then compute m and its uncertainty $\sigma(m)$, corrected for stellar contamination as in 8). We bin the results in half-magnitude intervals. The number counts (in units of number per half-magnitude per square degree) are then computed by dividing the number of galaxies in each bin by the survey area. This survey area includes a correction for crowding, the process by which faint galaxies go undetected because they happen to fall within the detection isophote of a much brighter object (see T97 for details of how this was done). The correction varies from about 30% (in the one or two frames that contain a supergiant galaxy like NGC 4889) to about 5% (in most fields).

10) The number counts were corrected for Galactic extinction using the HI maps of Burstein & Heiles (1982) and the colour conversions of Cardelli et al. (1989). The Galactic extinction is $A_B = 0.05$ mag for the core fields and $A_B = 0.03$ for the NGC 4839 field. Extinction from dust in Coma and the effects on the background galaxies of gravitational lensing by the cluster dark matter are assumed to be negligible (see Bernstein et al. 1995).

The numbers of galaxies that we detected in each bin are presented in Tables 3 and 4. Different fields had different m_L values because the seeing varied; this is why the numbers of fields in the last rows of the table are smaller than in the other rows. Our resulting magnitude – number count plots are shown in Figure 2 for the Coma core field and Figure 3 for the NGC 4839 field. The uncertainties are the quadrature sum of uncertainties from counting statistics and uncertainties from the isophotal corrections $\sigma(m)$. The uncertainties from counting statistics dominate at the bright end, and the uncertainties from isophotal corrections dominate at the faint end. Also shown in Figures 2 and 3 are the mean background counts for random sky fields (T97); it is clear from Figure 2 that for the Coma core region, the background contributes more to the total number counts at fainter magnitudes.

The luminosity function is computed by subtracting the background contribution from the number counts, and the uncertainty is computed taking into account the field-to-field variance in the background in addition to the errors described in the last paragraph.

The background counts are presented in T97; we use both the mean number counts and the field-to-field variance of the background computed there (corrected for differences in field size using Poisson statistics) in this work. The background fields studied in T97 comprise a total area of 132.4 arcmin² in B and 188.1 arcmin² in R imaged to $m = 25.5$ in both passbands, which is deeper than any of the Coma data presented here. The background data was treated in exactly the same way as the data in this work, as outlined earlier in this section. The background fields, like Coma, are at high Galactic latitude ($b > 30^\circ$) so that stellar contamination is small there too. We adopt the field-to-field variance measurements of Bernstein et al. (1995) in the R -band, as they have slightly better statistics than we do, and derive the B -band variance from the R -band variance using the measurements of Driver et al. (1994a; see T97 for details).

In converting apparent magnitudes to absolute magnitudes, we adopt a distance modulus of 34.83.

2.2.2 Computation of Colours

For each object described above, we compute the aperture magnitude m_a in an aperture of diameter $3''.0$. For the faint objects whose colours we will be measuring, we take the colour $B - R$ as $(m_a)_B - (m_a)_R$. Isophotal magnitudes are not used for computing colours because the detection isophotes are not the same in the different bands. The $3''.0$ aperture is large

enough that differential seeing between our B and R images and noise-induced subarcsecond offsets between the light centers of objects in the two images are negligible.

The above method fails to give accurate colours for bright galaxies if colour gradients are large. However, we will only present colours for galaxies with $R > 20.5$.

3 RESULTS AND DISCUSSION

3.1 Luminosity Functions

We present the LF for the Coma core field in Figures 4 (R -band) and 5 (B -band). The same general form of the LF is apparent in all the figures: a steep drop towards the bright end at $M_B < -21$, a shallow rise toward lower luminosities at intermediate magnitudes ($-20 < M_B < -16$), and a steep rise fainter than this. The statistics are good enough that the curvatures at both the bright and faint ends of the LF are highly significant – neither a power law nor a Schechter (1976) function provides an acceptable fit to the data.

The data presented in Figures 4 and 5 are also presented in Tables 5 and 6, along with the local LF slope, measured in four different ways. Here α is defined as the logarithmic slope of the LF: $\phi(L) \propto L^\alpha$ so that $N(M) \propto -\phi(L) \frac{dL}{dM} \propto 10^{-0.4(\alpha+1)M}$. We define $-0.4(\alpha_{mn}(M) + 1)$ as the slope at M of the best fitting polynomial of order m to the $2n + 1$ points in Figures 4(a) or 5(a), computed at 0.5 magnitude intervals, centered on M . The case $m = 1$ is a power-law fit. The error in α is mostly systematic; a good estimate of the true α is the median of the four values and a plausible estimate of the uncertainty in the true α is the range of the numbers.

The error bars get larger at fainter magnitudes because the background counts contribute more to the total counts at a rate faster than the field-to-field variance decreases with increasing magnitude. It is intriguing that the faintest point in the R -band is so low. We may be seeing a hint of a true turnover in the LF. An alternative explanation is that this is a normalization effect (recall that only 6 of the 16 fields that made up the mosaic are included in this point). It is therefore instructive to consider the counts in these 6 fields in isolation. For these 6 fields considered in isolation, in the $M_R = -11.11$ point, following background subtraction, we have 7_{-185}^{+190} galaxies, and in the $M_R = -11.61$ point we have 341_{-169}^{+103} galaxies. If the errors are Gaussian, the probability of there being more galaxies in the fainter point is than only 9.4% – this is significant, but only at the 1.7σ level.

Similar LFs have been seen by us, but only at the faint end, in Abell 262 and the NGC 507 Group (T97), and only at the bright end in Abell 665 and Abell 963 (Trentham 1997b). We can only see the faint-end of the LF in Abell 262 and the NGC 507 Group because these are poor clusters so that counting statistics at the bright end are poor so that we cannot constrain the LF. We can only see the bright-end of the LF in Abell 963 and Abell 665 because the clusters are distant ($z = 0.2$) and we cannot image them deeply enough to reach $M_B > -14$. In a separate paper (Trentham 1997c), we combine these results with others from the literature and show that all the LF shapes are consistent with each other to a high degree of precision and that the cluster LF appears to be universal.

The upturn in the LF occurs faintward of the magnitude where the LF in Virgo changes from being giant-dominated to dwarf-dominated ($M_B \sim -17$ for $H_0 = 75 \text{ km s}^{-1} \text{ Mpc}^{-1}$, which corresponds to $M_R \sim -18.5$ for dSph galaxies; Binggeli 1987). In both B and R , the LF is in fact quite shallow at this transition magnitude. This suggests that (i) either the transition occurs at different magnitudes in different environments, or (ii) the giant galaxy LF is decreasing by an amount only just less than the dwarf-galaxy LF is rising at the transition magnitude – hence a total galaxy LF that is gradually rising and almost

featureless. In Virgo, the type-specific LF has been measured (Sandage et al. 1985), and suggests that (ii) is the explanation there. If the cluster LF is universal, this would suggest that this explanation is valid here, too.

Neither Figure 4 nor Figure 5 shows a significant difference in the LF between the inner ($r < 200$ kpc) and outer ($r > 200$ kpc) regions of the cluster. The same parent LF (e.g., the composite LF of Trentham 1997c) can fit both LFs individually at a high level of confidence if the normalization is adjusted. The distribution of the dwarfs in the cluster is described in detail in Section 3.4. There we do see an apparent difference between the distributions of giants and dwarfs in the cluster at a low level, and we give possible explanations.

In Figures 4 and 5 we also present the LF of extreme low-surface-brightness (LSB) galaxies. How such galaxies are defined is described in the next section, but these very diffuse galaxies, while almost certainly cluster members, do not contribute most of the excess galaxies seen at faint magnitudes. At brighter magnitudes they contribute proportionately more to the LF ($\sim 60\%$ at $M_R = -17$ compared to $\sim 20\%$ at $M_R = -12$). This suggests that cluster dwarfs are easier to distinguish from background galaxies on morphological grounds alone at progressively brighter magnitudes.

The LF of the NGC 4839 Group is poorly constrained because the group is sufficiently diffuse that the ratio of members to background galaxies at a given apparent magnitude is low. The field-to-field variance of the background then causes the error bars to be large and we cannot measure the LF.

3.2 Scalelengths

In Figure 6, we present the m_I and r_1 values of all the objects we detect in the core field. These diagrams are similar to projections of the fundamental plane, except that the radius parameter is seeing convolved and the magnitude parameter is a measured isophotal one, not a computed total one. Lower surface-brightness galaxies have a larger r_1 for a given m_I . Stars are included – these have r_1 close to the seeing, and have the lowest r_1 of any objects of a given m_I . The thickness of the band of points at bright magnitudes and low r_1 gives a measure of the range of the seeing in our fields.

The solid line represents galaxies having the scalelengths of typical local dSphs as seen at the distance of Coma and observed under similar conditions to our data. The local dSph fundamental plane is not a tight correlation, and the scatter around this line is substantial. The figure suggests that the excess objects we find at $R > 19$ and $B > 20$ (galaxies with $M_R > -15.83$ and $M_B > -14.83$ if they are in the cluster) in Figures 4 and 5 have scalelengths consistent with those of dSphs.

We cannot determine which points in Figure 6 refer to cluster galaxies and which to background galaxies. Comparison between the solid and dotted lines suggests that for much of our magnitude range of interest, cluster dwarfs have scalelengths similar to background galaxies. Therefore a detailed quantitative analysis of exactly which region of the fundamental plane is occupied by dwarfs is not possible with our data. A natural follow-up program would be a velocity survey of the faint galaxies with $B > 20$. Then we could identify which galaxies are cluster members and see where they lie in the magnitude–radius projection of the fundamental plane (higher resolution imaging data would be required too).

The figure also suggests that in Coma, lower surface-brightness galaxies do not contribute proportionately more to the LF at fainter magnitudes. We also found this to be true in Abell 262 and the NGC 507 Group (T97). We find a number of galaxies whose surface brightnesses are lower than those of any background galaxies i.e., those above the dashed line in the figure. In Figures 4 and 5 we present the LFs for these objects in panel (d). That these galaxies have a flat luminosity function confirms the earlier statement that the LSB galaxies do not contribute more to the LF at fainter magnitudes. This statement is, however, subject to the important caveat that our detection efficiency of LSB galaxies decreases at fainter magnitudes, so that such galaxies might exist and not be seen. However, we do not find proportionately more galaxies of lower surface-brightnesses within the surface-brightness range where we can detect with 100% completeness, on going to fainter magnitudes i.e. there are not many points near the points with the largest r_1 at the faintest m_I that we do observe. This of course does not rule out the existence of a population of **very** low surface-brightness objects at $20 < m < 24$ ($-15 < M_R < -11$ in Coma), but such objects have not turned up in substantial number in any known environment. The faintest giant galaxies known, with central surface-brightnesses of $\mu_R \sim 26.5$ mag arcsec $^{-2}$ (e.g., GP1444, Davies et al. 1988), would have been marginally detected here if they were in Coma.

Although the faintest galaxies we detect have scale lengths consistent with those we would expect of local dSphs placed in Coma, this is not sufficient information for us to conclude that they **are** dSphs. This is because the dSph and dIrr fundamental planes overlap (Kormendy 1987, Binggeli 1994). We need additional information, in particular colours, to distinguish between these two types of galaxies. This is discussed in the next section.

3.3 Colours

Figure 7 presents the colour distribution of galaxies with $20.5 < R < 22.5$, computed as described in Section 2.2.2. We selected this magnitude range because we want to examine the properties of the galaxies where the LF is steeply rising. We only consider galaxies with $R < 22.5$ so as to ensure completeness except for galaxies with $B - R > 2.3$, which is much redder than the colour of old stellar populations at the distance of Coma.

Figure 7(b) shows the colour distribution after the estimated contribution from the background has been subtracted. That the histogram is approximately zero at red colours, where the cluster contribution is presumably negligible, is encouraging that the subtraction is reliable. This figure suggests that the Coma dwarfs have a colour distribution that is strongly peaked at $B - R = 1.3$. This would suggest that they are dSphs (dIrr's have colours bluer than this: $B - R < 1.1$).

Local dSphs have a substantial range of colours (see Hodge 1989, Trentham 1997b). The main parameters determining the colour (Hodge 1989, 1994) are the star formation history (galaxies that have current or recent star formation are bluer) and the metallicity (higher metallicity stellar systems are redder). A value of $B - R = 1.3$ is near the blue end of the colours seen for local dSphs and suggests that the Coma dwarfs might have undergone more recent star formation than their redder counterparts in Virgo (Caldwell 1983) or Abell 262 (T97). That the distribution is so peaked suggests that most of these dwarfs would have had similar star-formation histories to each other (and probably similar metallicities too). If the Coma cluster really is the result of a recent merger of two smaller clusters, as suggested by its two large central galaxies and absence of a cooling flow (Stewart et al. 1984), perhaps star formation was triggered at this time in most low-mass galaxies, which might have had somewhat more gas than they do now, by the rapidly changing gravitational fields during the merger.

Figures 7(c) and 7(d) suggest a radial colour gradient that is much smaller than that measured by Secker (1996, hereafter S96) for brighter dwarf galaxies. We find, in the units of S96, $\frac{\Delta(B-R)}{\Delta \log_{10} r} = -0.0284 \pm 0.0208$. S96 found $\frac{\Delta(B-R)}{\Delta \log_{10} r} = -0.08 \pm 0.02$ for Coma dSph's with $15.5 < R < 20$. What these results suggest is that colour gradients get smaller on going to fainter magnitudes. This could be because star formation is turned off more efficiently on lower mass systems as they enter the cluster environment. Alternatively, the difference between the S96 results and ours could be due to contamination of his sample by red low-luminosity normal elliptical galaxies (like M32) near the cluster center. Dressler (1980) showed that ellipticals prefer high density environments. Such galaxies do not exist or are extremely rare as faint as $M_R = -14.3$ ($R = 20.5$ in Coma), so our sample will not suffer from this problem. S96 also found that the mean colour of the $15.5 < R < 20$ dwarfs at $1'$ from the cluster center is $B - R = 1.46 \pm 0.02$, slightly redder than the mean value we find for the $20.5 < R < 22.5$ sample of $B - R = 1.34 \pm 0.01$ (adopting the same colour criterion as Secker for inclusion in the computation: $1.05 < B - R < 1.6$; note that there is no significant colour gradient in our sample). This does not, however, help to distinguish between the two possibilities above.

For the NGC 4839 group, as in Section 3.1, no useful conclusions can be made because the galaxy density relative to the background is too low and counting statistics dominate following subtraction.

The LSB galaxy colour distribution (Figure 7(f)) is also peaked at $B - R = 1.3$. These too may be dSph galaxies; Figure 6 does not rule this out, as the scatter around the dSph line is large (see Section 3.2).

3.4 Radial Distributions

Figure 8 shows how the galaxies described in the previous section ($20.5 < R < 22.5$) are spatially distributed in the cluster. Brightness encodes the number of galaxies (cluster plus background) in the above magnitude range in a 170 arcsecond aperture. The aperture size is chosen as a compromise. Very small apertures would result in very poor counting statistics. Very large apertures would result in such bad edge effects that we could not present a figure like Figure 8 over a significant area of the cluster. The values in neighbouring pixels are not independent because of the aperture size; they are only truly independent in regions more than 340 arcseconds apart; the degree of coupling between the values falls with the distance between the pixels.

In Figure 9 (upper panel), we plot the radial average of the numbers in Figure 8, where the radius is measured from the center of NGC 4874 (the X-ray emission is centered on this galaxy). The large aperture smooths features in the counts distribution that are smaller than the aperture size (73 kpc at the distance of Coma). Consequently, as outlined in the previous paragraph, adjacent points here are not statistically independent; neither are the error bars, which are in part due to counting statistics. In the lower panel of Figure 9, we show the corresponding distribution for the brighter galaxies, measured in the same way. The background contribution is negligible in the lower panel.

Figure 9 shows that the projected distribution of galaxies with $20.5 < R < 22.5$ is high at the center and then drops rapidly towards the background value between 300 and 500 arcseconds (130 and 220 kpc). The true drop in the distribution may be sharper still, because of the smoothing due to the large aperture size. The radial distribution of the brighter galaxies (lower panel) shows a much more shallow drop (density $\sim r^{-1}$; similar results have been obtained by other authors – see e.g. Thompson & Gregory 1993). Figure 8

shows that the form of the distribution for the fainter galaxies is caused by two condensations of galaxies, each about 300 kpc from NGC 4874.

The steep drop in the upper panel of Figure 9 and the condensations seen in Figure 8 are interesting, but we stress that this is not a big effect: the excess galaxies seen in this central 300 kpc is approximately 30% above the background. The background easily fluctuates by this amount on the scales shown in Figure 8. If the galaxies in the condensations in Figure 9 are cluster galaxies, this would suggest (i) that they have orbits which are more elongated towards the observer than the orbits for the giant galaxies, or (ii) that as a population, they have a smaller velocity dispersion than do the larger galaxies, and so are more confined to the core. If either of these is an explanation for what we see, then this provides a very important constraint on the formation of the Coma cluster. Specifically it would mean that the time since the cluster formed (say, from a merger of two subclusters, as discussed in the previous section) is short compared to the cluster crossing time, or else the cluster would have virialized and such a structure would not have survived. In Section 3.2, we suggested obtaining velocities for the faintest dwarfs we see there. The same measurements would tell us whether the condensations that we see in Figure 8 are due to cluster or background galaxies, and would be able to distinguish between possibilities (i) and (ii) above, if they were cluster galaxies.

3.5 Summary and comparison with previous work

We have obtained a reasonably complete description of the dwarf galaxy population in Coma down to $R \sim 24$. A number of important questions remain, but a velocity survey of the central region of the cluster down to $R = 24$ would be able to address almost all of these. Such a program will shortly be possible with the advent of multi-object spectrographs on 8 m and 10 m telescopes.

We find a dwarf galaxy luminosity function that is steeply rising ($\alpha \sim -1.7$) at faint magnitudes. At brighter magnitudes, the LF is flatter, with a shape that agrees well with most previous determinations. In Table 7 we list a number of previous surveys and present the LFs from these surveys in Figure 10. A survey which was only complete to $M_B = -18$ or brighter would suggest a value of $\alpha \sim -1$ at the faint-end (e.g. Godwin & Peach 1977, Lugger 1986) and one complete to $M_B \sim -15$ would suggest $\alpha \sim -1.4$ (Thompson & Gregory 1993). By going deeper, we convincingly see that the LF steepens. In the field studied by Bernstein et al. (1995), this effect was masked by an even steeper contribution from globular clusters in the halo of NGC 4874 at the faintest magnitudes. This is less of a problem for us (i) because our survey covers a larger area, and (ii) because it excludes the halos of galaxies like NGC 4874 which have substantial globular cluster populations. If such galaxies also have particularly high dwarf galaxy satellite populations, we miss those too, but careful inspection of our data does not suggest that this is the case. The slope of our LF for $-14.5 < M_R < -12.5$ is slightly steeper than that ($\alpha = -1.41$) measured by SH96. Their measurement is not significantly different from our best value of α in this range, given the (mostly systematic, see Section 3.1 and Table 5) uncertainties. As stated in the introduction, SH96 made completeness corrections in their faintest points (although they were only 20% at most before background subtraction). Most of our simulations suggest that these corrections can be very unstable; for example, they depend critically on the sizes of galaxies being corrected for. This might lead to systematic uncertainties in the three faintest points of SH96 that are larger than the random errors that they estimate. Then it might be possible to reconcile their data with a slightly steeper α . In any case, this difference is not huge, and it is encouraging that their LF is so similar to ours everywhere except at their three

faintest points. Finally, Figure 10 suggests that the slope of $\alpha = -1.8$ for $-19 < M_V < -15$ found by Lobo et al. (1996) is somewhat steeper than the slope seen in the other surveys.

Our faintest point in the R -band is very low ($M_R \sim -11$). This might be a normalization effect, or it might be suggestive of a turnover in the LF (most theories suggest a turnover at faint magnitudes because of the suppression of star formation in low mass galaxies; Efstathiou 1992, Chiba & Nath 1994, Thoul & Weinberg 1995).

The dwarf galaxies in Coma have colours and scalelengths that are characteristic of dSph galaxies. The scale-length measurements extend the results of Karachentsev et al. (1995) to fainter magnitudes. The colour distribution of galaxies with $-14.3 < M_R < -12.3$ is strongly peaked at $B - R = 1.3$, suggesting some homogeneity in their recent star-formation histories. This is slightly bluer than what S96 found for the brighter dwarfs; the colour gradient for the fainter galaxies is also weaker.

The faintest dwarfs also seem to be more confined to the cluster center than the giant galaxies. Alternatively, this measurement may in part or whole be due to background clustering; velocity measurements should easily distinguish between these possibilities.

We cannot make any detailed conclusions about the dwarf galaxy population in the NGC 4839 group because the galaxy density is too low there relative to the background.

ACKNOWLEDGMENTS

This research has made use of the NASA/IPAC extragalactic database (NED) which is operated by the Jet Propulsion Laboratory, Caltech, under agreement with the National Aeronautics and Space Administration.

REFERENCES

- Abell G. O., 1958, ApJS, 3, 211
Babul A., Ferguson H. C., 1996, ApJ, 458 100
Bernstein G. M., Nichol R. C., Tyson J. A., Ulmer M. P., Wittman D., 1995, AJ, 110, 1507
Binggeli B., 1994, in Meylan G., Prugneil P., ed., ESO Conference and Workshop Proceedings No. 49: Dwarf Galaxies. European Space Observatory, Munich, p. 13
Biviano A., Durret F., Gerbal D., Le Fevre O., Lobo C., Mazure A., Slezak E., 1995, A&A, 297, 610
Briel U. G., Henry J. P., Bohringer H., 1992, A&A, 259, L31
Burstein D., Heiles C., 1982, AJ, 87, 1165
Caldwell N., 1983, AJ, 88, 804
Cardelli J. A., Clayton G. C., Mathis J. S., ApJ, 345, 245
Chiba M., Nath B. B., 1994, ApJ, 436, 618
Coleman G. D., Wu C-C., Weedman D. W., 1980, ApJS, 43, 393
Davies J. I., Phillipps S., Disney M. J., 1988, MNRAS, 231, 69p
Dressler A., 1980, ApJ, 236, 351
Driver S. P., Phillipps S., Davies J. I., Morgan I., Disney M. J., 1994a, MNRAS, 266, 155
Driver S. P., Phillipps S., Davies J. I., Morgan I., Disney M. J., 1994b, MNRAS, 268, 393
Efstathiou G., 1992, MNRAS, 256, 43p
Godwin J. G., Metcalfe N., Peach J. V., 1983, MNRAS, 202, 113
Godwin J. G., Peach J. V., 1977, MNRAS, 181, 323
Hodge P. W., 1989, ARAA, 27, 139

- Hodge P., 1994, in Munoz-Tunon C., Sanchez F., ed., *The Formation and Evolution of Galaxies*. Cambridge University Press, Cambridge, p. 1
- Hughes J. P., Gorenstein F., Fabricant D., 1988, *ApJ*, 329, 82
- Jarvis J. F., Tyson J. A., 1981, *AJ*, 86, 476
- Jones L. R., Fong R., Shanks T., Ellis R. S., Peterson B. A., 1991, *MNRAS*, 249, 481.
- Karachentsev I. D., Karachentseva V. E., Richter G. M., Vennik J. A., 1995, *A&A*, 296, 643
- Kormendy J., 1985, *ApJ*, 295, 73
- Kormendy J., 1987, in Faber S. M. ed., *Nearly Normal Galaxies*. Springer-Verlag, New York, p. 163
- Landolt A. U., 1992, *AJ*, 104, 340
- Lobo C., Biviano A., Durret F., Gerbal D., Le Fevre O., Mazure A., Slezak E., 1996, preprint astro-ph/9605194
- Lugger P., 1986, *ApJ*, 303, 535
- Rood H. J., Baum W. A., 1967, *AJ*, 72, 398
- Sandage A., Binggeli B., Tammann G. A., 1985, *AJ*, 90, 1759
- Schechter P., 1976, *ApJ*, 203, 297
- Schombert J. M., 1988, *ApJ*, 328, 475
- Secker J., 1996, *ApJ*, 469, L81 (S96)
- Secker J., Harris W. E., 1996, *ApJ*, 469, 628 (SH96)
- Stewart G. C., Fabian A. C., Jones C., Forman W., 1984,
- Soltan A., Henry J. P., 1983, *ApJ*, 271, 442
- Thompson L. A., & Gregory S. A., 1993, *AJ*, 106, 2197
- Thoul A. A., Weinberg D. H., 1995, *ApJ*, 442, 480
- Trentham N., 1997a, *MNRAS*, 286, 133
- Trentham N., 1997b, *MNRAS*, submitted
- Trentham N., 1997c, *MNRAS*, submitted
- Valdes F., 1982, *Proc. SPIE*, 331, 465
- Valdes F., 1989, in Grosbol P. J., Murtagh F., Warmels R. H., ed., *ESO Conference and Workshop Proceedings No. 31: Proceedings of the 1st ESO/St-ECF Data Analysis Workshop*. European Space Observatory, Munich, p. 35
- van den Bergh S., 1976, *ApJ*, 206, 883
- White S. D. M, Kauffmann G., in Munoz-Tunon C., Sanchez F., eds., *The Formation and Evolution of Galaxies*. Cambridge University Press, Cambridge, p. 455
- Zabludoff A. I., Huchra J.P., Geller M. J., 1990, *ApJS*, 74, 1

FIGURE CAPTIONS

Figure 1. The Palomar Sky Survey image of the Coma cluster. The whole image is 80 arcminutes square, with North up and East to the left. The two bright central galaxies are NGC 4874 (to the west) and NGC 4889. The next two brightest galaxies are the anaemic (van den Bergh 1976) spiral galaxy NGC 4921, 18 arcminutes to the southeast of NGC 4889, and NGC 4839, 41 arcminutes to the southwest of NGC 4874.

The boxes represent our survey areas. The large box to the northeast is the Coma core region; it covers 674 square arcminutes, and we surveyed 97% of it. The smaller box to the southwest is the NGC 4839 field.

Figure 2. Number counts versus magnitude for the Coma core region in the R -band (upper panel) and B -band (lower panel). The dashed lines are the mean background counts from T97 ($\log_{10} N = 0.376R - 4.696$ and $\log_{10} N = 0.488B - 7.702$). These lines come from a fit to the number counts in T97 for $21 < m < 25$ in both B and R . For $m < 21$ the mean background counts shown in Figure 6 of T97 are consistent with these lines but the errors in the measurements there are large; any systematic deviation of the mean counts from these lines is negligible compared with the field-to-field variance of the background. Brighter than $B = 17$ and $R = 16$, background contamination in the Coma fields is negligible.

Figure 3. As Figure 2, but for the NGC 4839 field.

Figure 4. The R -band luminosity function of the Coma core region outlined in Figure 1, computed from the data in Figure 2 as described in the text. The four panels are: (a) the LF for the whole field; (b) the LF for the inner 200 kpc, adopting the center of NGC 4874 as the cluster center; (c) the LF of the remaining part of the field not included in (b); (d) the LF for the extreme-low-surface-brightness galaxies, defined as galaxies whose surface brightnesses are lower than that of any field galaxies having the same total magnitude.

Slopes corresponding to different values of α are shown in panel (a). The error bars represent the quadrature sum of uncertainties from counting statistics, measurements of the total magnitudes, and uncertainty from the field-to-field variance of the background.

Figure 5. As Figure 4, but for the B -band

Figure 6. The isophotal magnitude m_I and first-moment light radius r_1 of all detected objects in the Coma core field. The solid line shows where typical local dSphs placed at the distance of Coma would lie; the scatter around this line is, however, large. The dashed line shows the upper envelope of the region occupied by background galaxies (see T97). The line is higher relative to the dSph line in the B -band than in the R -band because the lowest-surface-brightness field galaxies are blue. The dotted-dashed lines represent the line below which we detect all zero-ellipticity exponential galaxies in the absence of other brighter galaxies. The lines represent the median such line for all the images in our survey; the differences are small except at the very faint end. A few objects above the line are seen; most are either very elongated low surface-brightness galaxies, or galaxies that we happen to detect despite our not being complete in this region of the diagram.

Figure 7. Colour distributions of the galaxies with $20.5 < R < 22.5$ ($-14.3 < M_R < -12.3$ if the galaxies are in Coma) computed as described in Section 2.2.2 using magnitudes in a $3''.0$ diameter aperture. When deciding whether a galaxy is included, we see if the aperture magnitude satisfies the above criterion (except for in panel (f), where we use the isophotal magnitude, as this is a better approximation to the total magnitude in this case). Only objects labeled “galaxy” in both B and R FOCAS catalogs were included; this makes stellar contamination negligible. Cluster and background were treated the same way throughout the analysis. The background data come from T97.

The panels are: (a), raw data for the entire core field, prior to background subtraction; (b), histogram for the entire core field with a background contribution subtracted; (c), as (b) but only for galaxies with $r < 200$ kpc; (d), as (b) but for galaxies with $r > 200$ kpc; (e), the background-subtracted histogram for the NGC 4839 field, and (f) the LSB galaxies (no background subtraction is necessary here).

The histograms are complete to $B-R = 2.3$ (a giant elliptical in Coma has $B-R \sim 1.9$; Coleman et al. 1980). The vertical error bars in each bin are approximately equal to the Poisson (\sqrt{N}) errors; horizontal error bars are small.

Figure 8. The number of galaxies with $20.5 < R < 22.5$ in a 170 arcsecond radius aperture as a function of position in the Coma cluster. The region of the cluster core shown here is 1080 arcseconds square; north is up and east is to the left. The positions of NGC 4874 (X) and NGC 4889 (Y) are shown. The colour coding is shown below.

Figure 9. The upper panel shows the radial average of the number of galaxies having $20.5 < R < 22.5$ within a 170 arcsecond radius aperture, as a function of distance from the cluster center, which we define as the center of NGC 4874. The lower panel shows the corresponding plot for the brighter galaxies ($15 < R < 19$). The mean backgrounds are 59.1 (the dotted line) in the upper panel and 1.13 in the lower panel. One arcminute corresponds to 26 kpc in Coma.

Figure 10. The luminosity functions for the surveys listed in Table 7. The normalizations are appropriate to each survey and are only equal for two surveys covering the same area. Surveys covering larger area generally have lower normalizations because they contain a bigger contribution from the outer regions of the cluster, where the galaxy density is low.

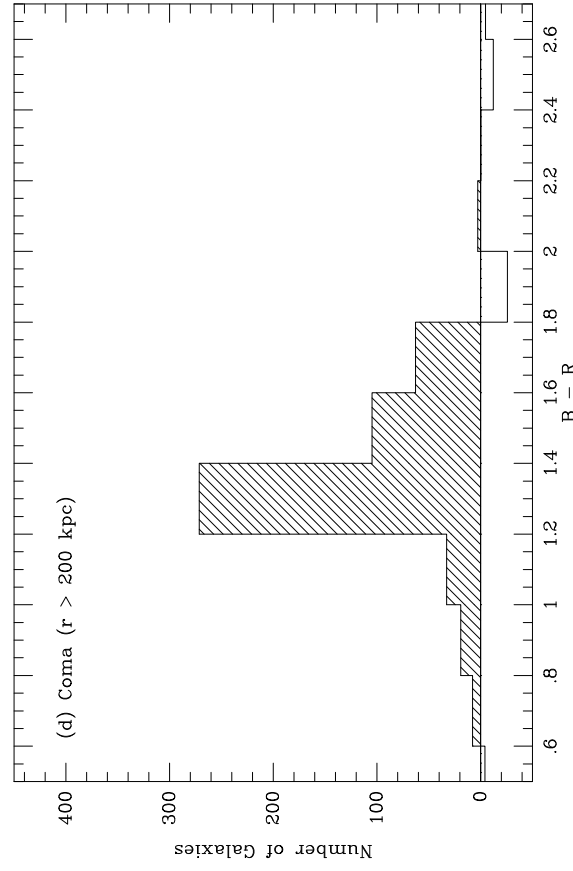
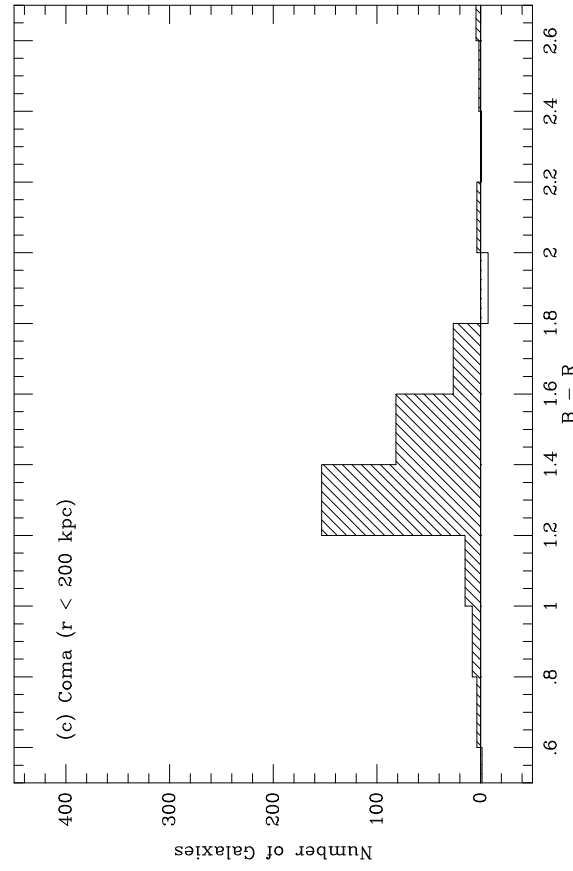
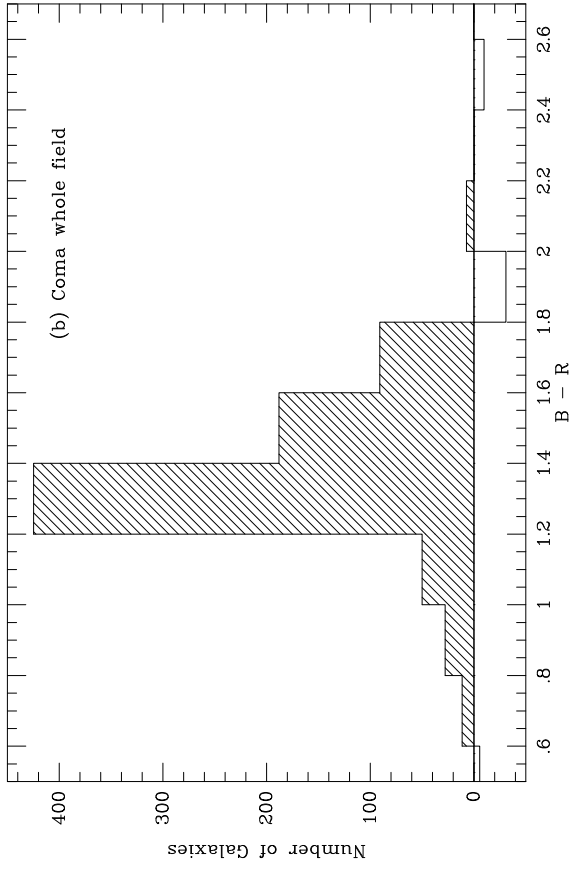
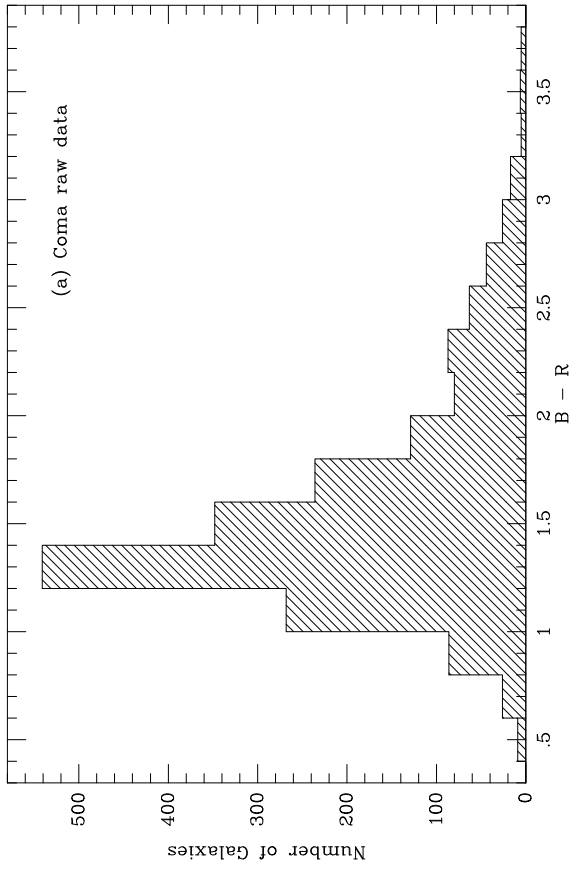


Table 1
Properties of the Coma Cluster (Abell 1656)

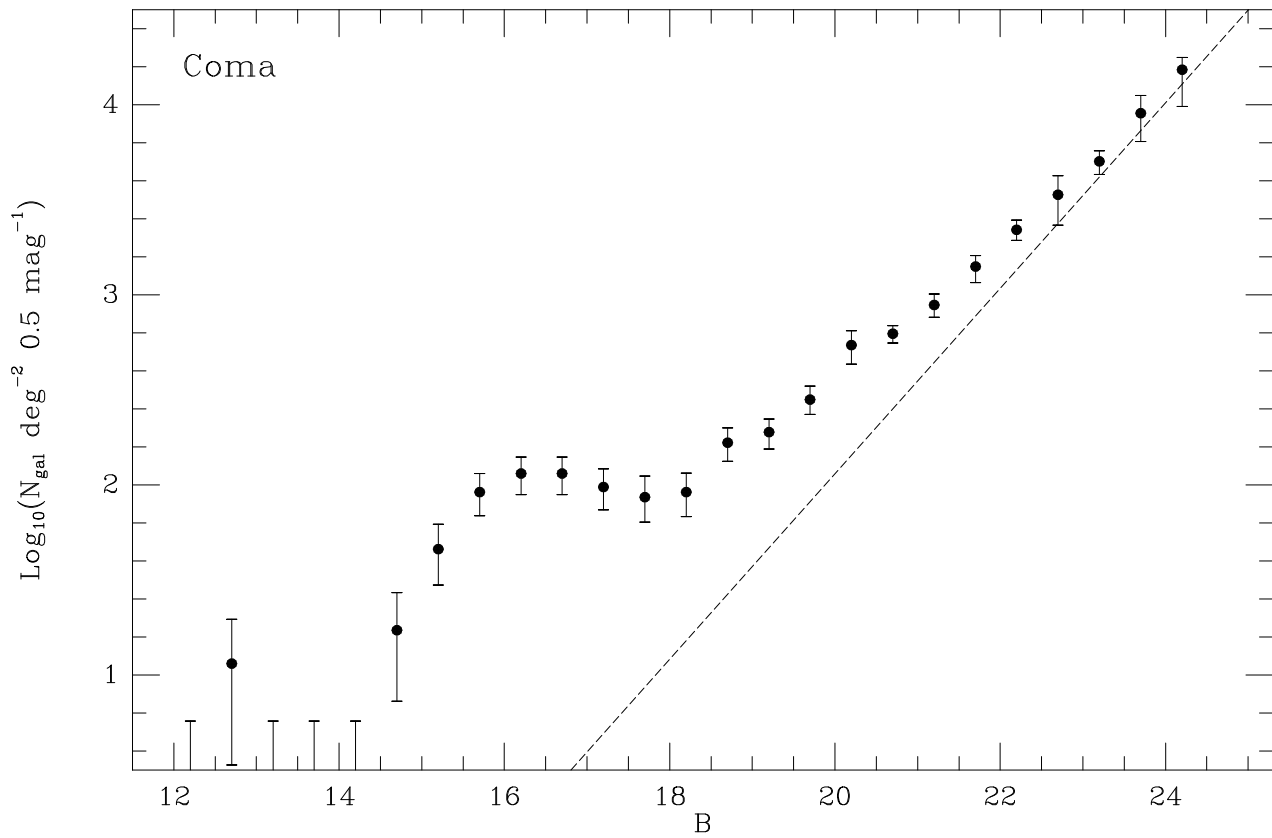
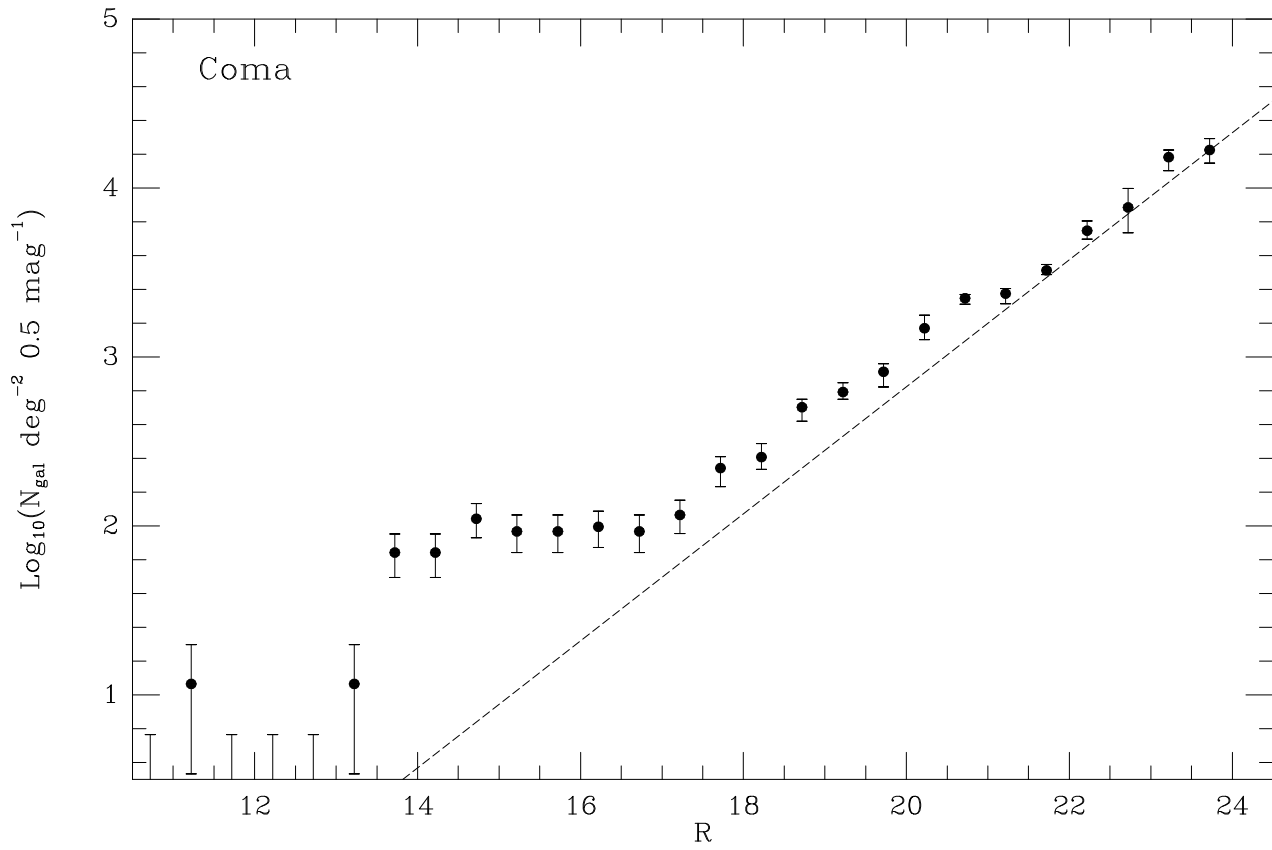
Richness (1)	z	σ km s ⁻¹	L_x erg s ⁻¹	A_B (8) mag	Σ_c g cm ⁻²
2	0.023	1010 (2)	3.7×10^{44} (3) [†]	0.05 (4)	4.0

Symbols: z = redshift; σ = velocity dispersion; L_x = X-ray luminosity; A_B = B -band Galactic extinction along our line of sight; Σ_c = critical surface density for gravitational lensing of distant sources.

[†] 2 – 10 keV Luminosity

$H_0 = 75$ km s⁻¹ Mpc⁻¹ and $\Omega_0 = 1$ assumed.

References: (1) Abell 1958; (2) Zabludoff, Huchra & Geller 1990; (3) Soltan & Henry 1983; (4) Burstein & Heiles 1982.



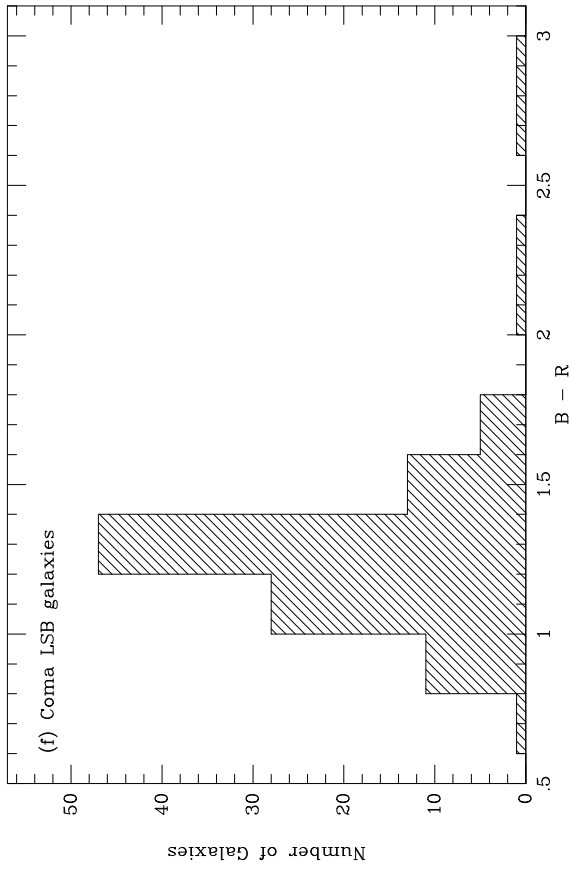
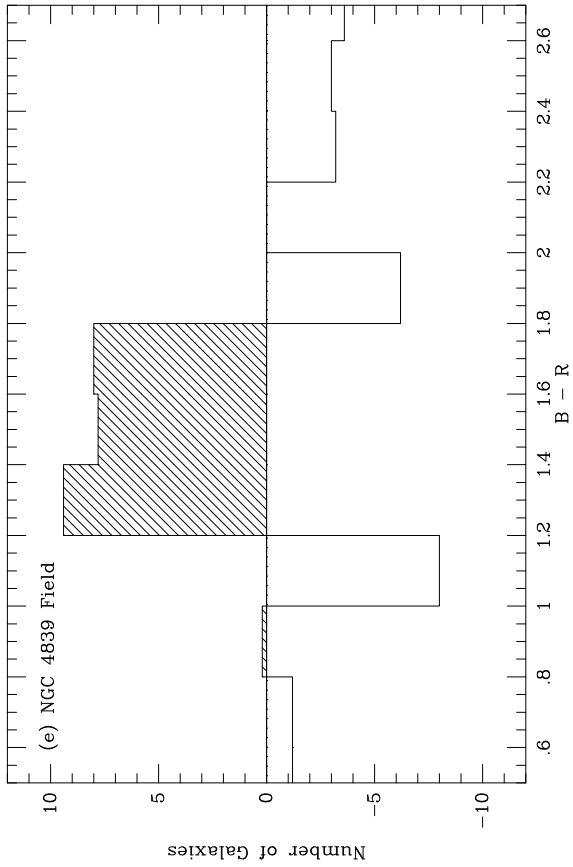


Table 2**Galaxies with excluded halos due to globular cluster contamination**

Galaxy	m_B	Type	V km s ⁻¹	α (1950)	δ (1950)	Excluded area sq. arcmin
NGC 4874	12.6	cD	7176	12 ^h 57 ^m 11.0 ^s	28°13'46''	2.24
NGC 4860	14.6	E	7864	12 ^h 56 ^m 39.1 ^s	28°23'35''	0.33
NGC 4908	14.7	E	8804	12 ^h 58 ^m 26.9 ^s	28°18'44''	0.11*
NGC 4869	14.8	E	6788	12 ^h 56 ^m 58.6 ^s	28°10'51''	0.59
NGC 4873	15.1	S0	5848	12 ^h 57 ^m 07.7 ^s	28°15'10''	0.24
IC 3959	15.2	E	7053	12 ^h 56 ^m 43.1 ^s	28°03'13''	0.35
RB 268	15.6	S0	7790	12 ^h 56 ^m 48.9 ^s	28°20'45''	0.43
RB 038	15.7	S0	6812	12 ^h 57 ^m 13.3 ^s	28°15'23''	0.27

The columns are: galaxy name (the RB numbers are from Rood & Baum 1967); blue magnitude m_B ; galaxy morphological type; heliocentric radial velocity V ; right ascension α ; declination δ ; the area of the region that we have excluded around the galaxy because of globular cluster contamination.

The data in this table comes from the NASA/IPAC extragalactic database (NED), excepting the last column. The reader is referred there for the original sources. We do not use our own magnitudes because most of the galaxies are not completely contained in a single CCD frame so that the magnitudes we measure can be unreliable.

*Most of this galaxy is not in our survey area. This represents the area we have subtracted from the part of the galaxy that is.

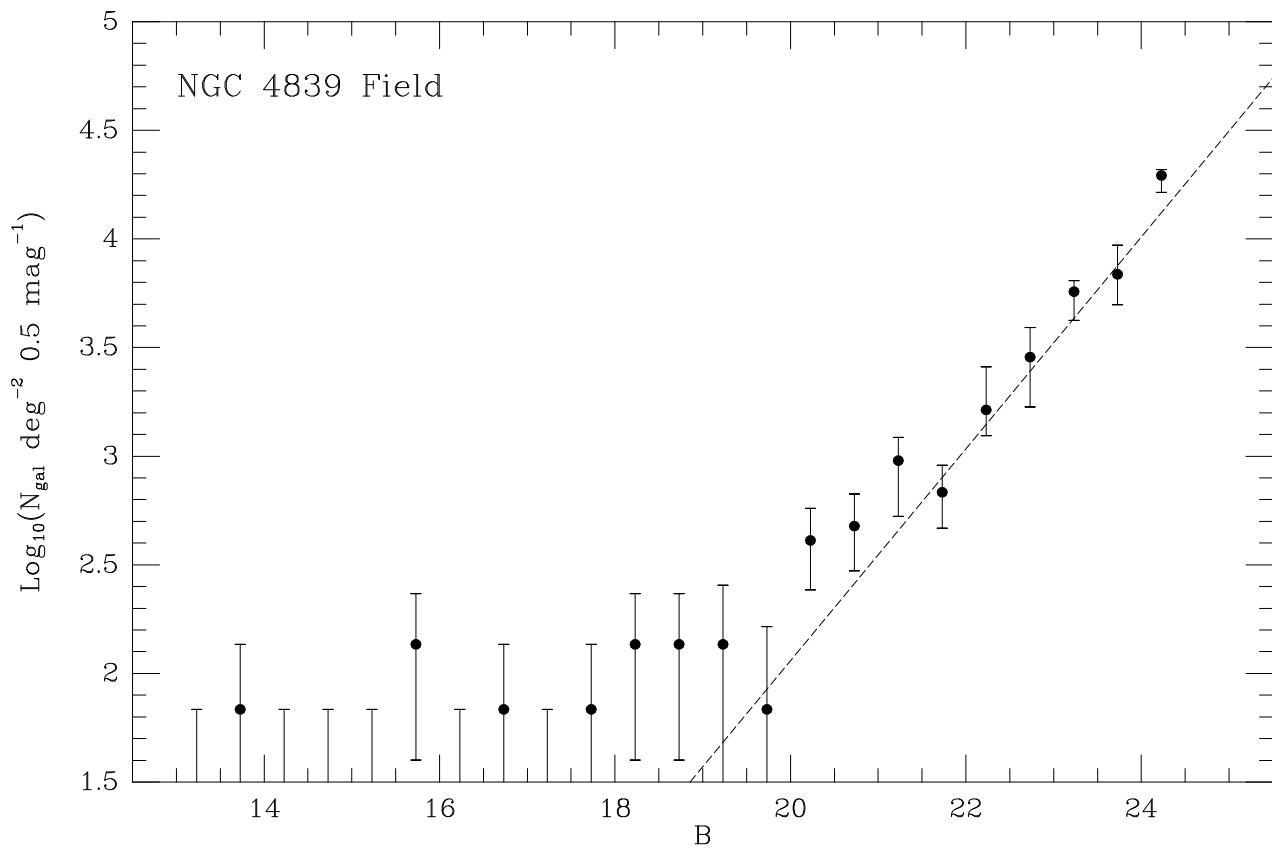
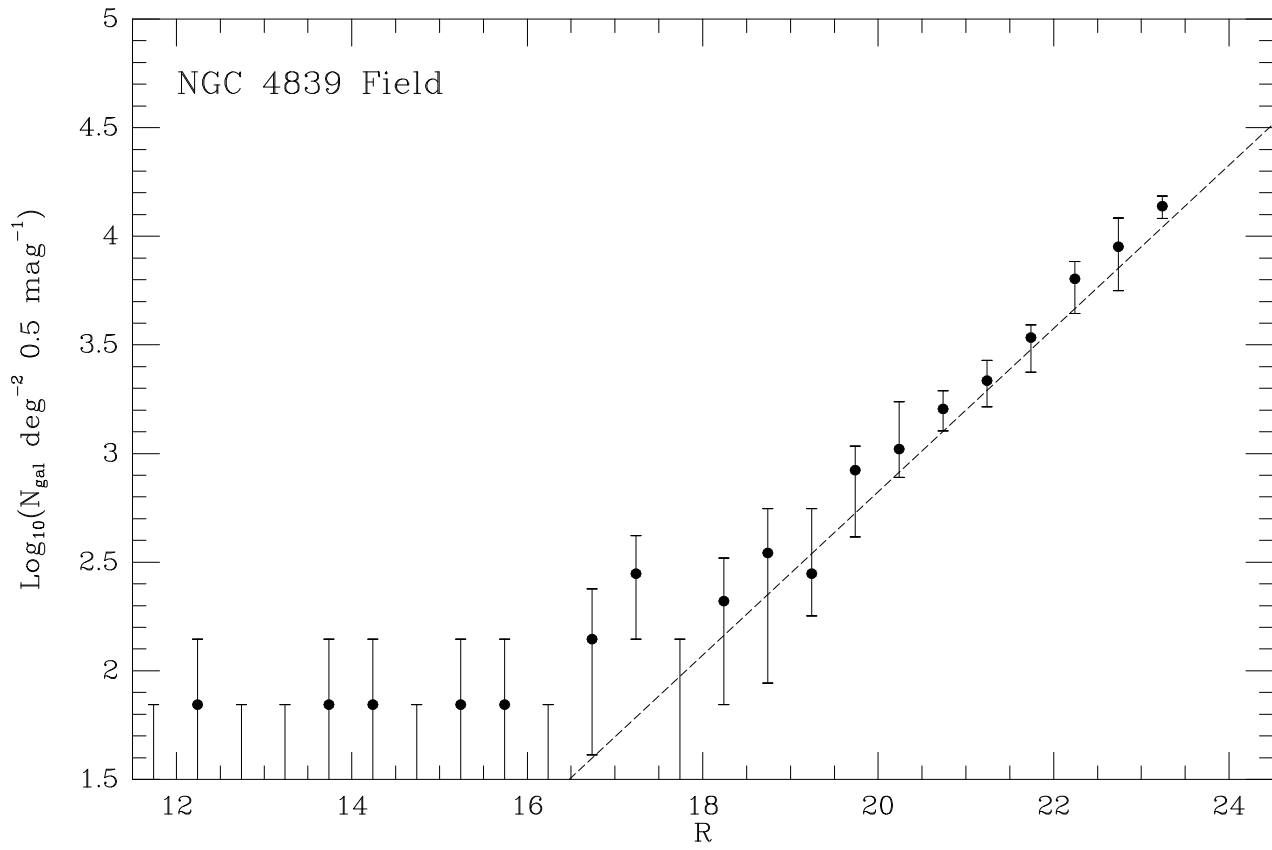


Table 3
R band observations

R	Number of Fields	N_{gal}	N_{bkg}	$(\frac{\Delta N}{N})_{\text{bkg}}$
		Measured	Predicted	Predicted
11.22	16	2 ± 1.4	0.1	0.90
11.72	16	0	0.1	0.84
12.22	16	0	0.1	0.77
12.72	16	0	0.2	0.71
13.22	16	2 ± 1.4	0.3	0.65
13.72	16	12 ± 3.5	0.5	0.60
14.22	16	12 ± 3.5	0.8	0.55
14.72	16	19 ± 4.4	1.2	0.49
15.22	16	16 ± 4.0	1.9	0.45
16.72	16	16 ± 4.0	2.9	0.40
16.22	16	17 ± 4.1	4.4	0.36
16.72	16	16 ± 4.0	6.8	0.32
17.22	16	20 ± 4.5	10.5	0.28
17.72	16	$38^{+6.2}_{-8.6}$	16.1	0.25
18.22	16	$44^{+8.9}_{-6.6}$	24.9	0.21
18.72	16	$87^{+10.1}_{-15.2}$	38.4	0.18
19.22	16	$107^{+14.4}_{-10.3}$	59.1	0.16
19.72	16	$141^{+16.2}_{-26.8}$	91.2	0.13
20.22	16	$255^{+49.7}_{-36.7}$	141	0.11
20.72	16	$383^{+20.0}_{-30.2}$	217	0.09
21.22	16	$408^{+29.9}_{-51.1}$	334	0.07
21.72	16	$560^{+46.5}_{-30.3}$	515	0.06
22.22	16	964^{+133}_{-104}	794	0.05
22.72	16	1325^{+386}_{-391}	1224	0.04
23.22	15	2459^{+247}_{-418}	1746	0.03
23.72	6	1084^{+185}_{-180}	1077	0.04

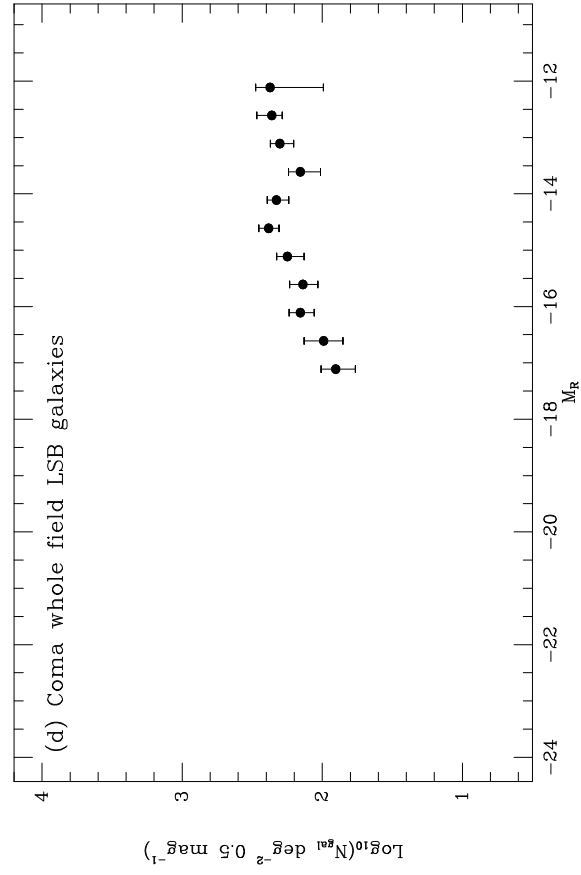
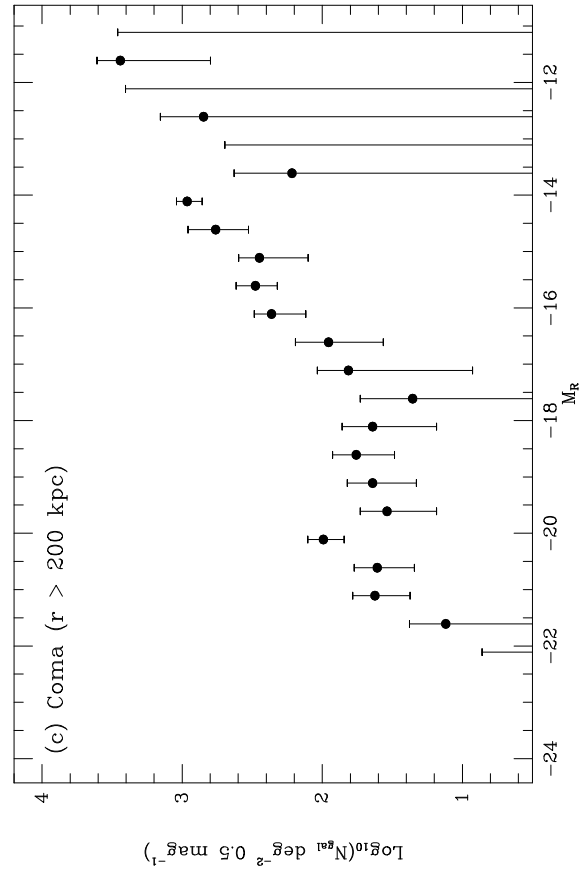
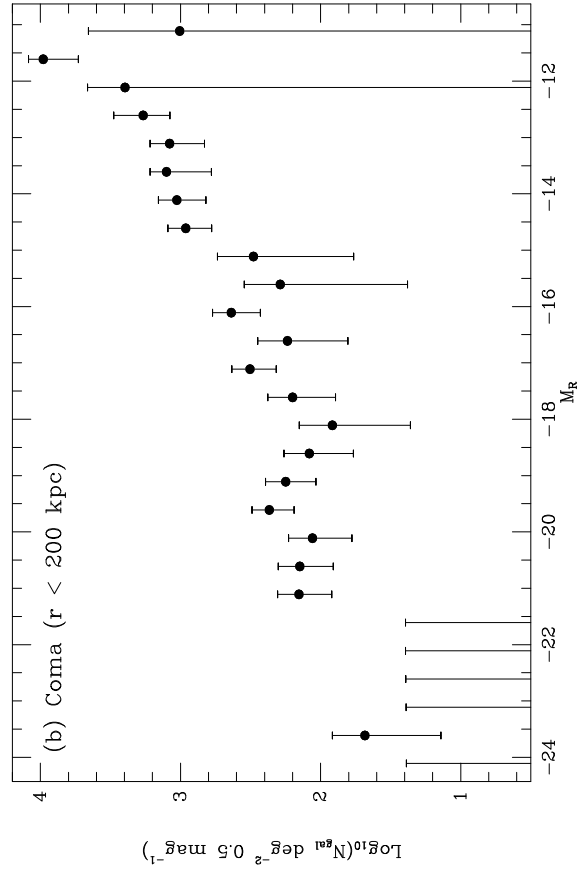
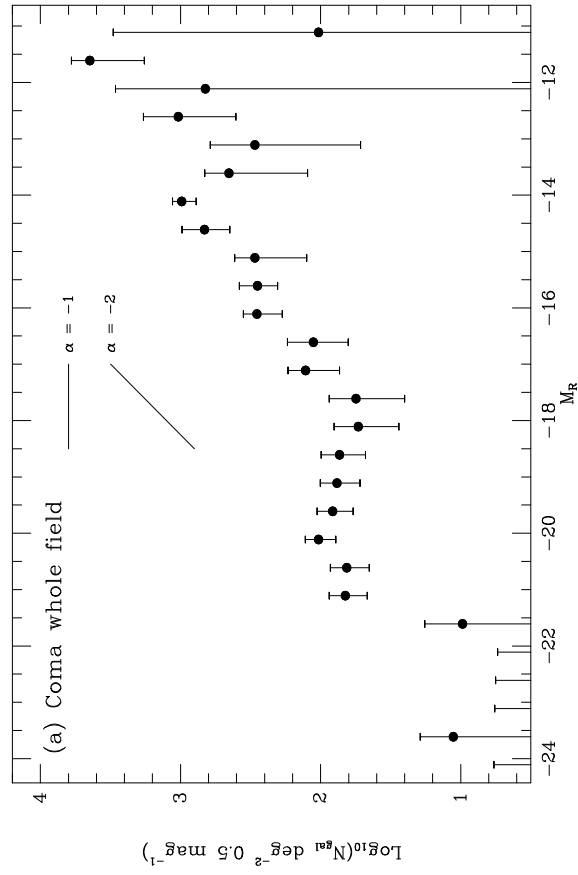


Table 4
B band observations

B	Number of Fields	N_{gal}	N_{bkg}	$(\frac{\Delta N}{N})_{\text{bkg}}$
		Measured	Predicted	Predicted
12.7	16	2 ± 1.4	0.0	0.91
13.2	16	0	0.0	0.84
13.7	16	0	0.0	0.78
14.2	16	0	0.0	0.72
14.7	16	3 ± 1.7	0.1	0.66
15.2	16	8 ± 2.8	0.1	0.60
15.7	16	16 ± 4.0	0.2	0.55
16.2	16	20 ± 4.5	0.3	0.50
16.7	16	20 ± 4.5	0.5	0.45
17.2	16	17 ± 4.1	0.9	0.40
17.7	16	$17^{+4.1}_{-4.6}$	1.5	0.36
18.2	16	$16^{+4.1}_{-4.1}$	2.6	0.32
18.7	16	$29^{+5.5}_{-5.7}$	4.6	0.28
19.2	16	$33^{+5.7}_{-6.1}$	8.1	0.25
19.7	16	$49^{+8.6}_{-8.1}$	14.2	0.21
20.2	16	$95^{+17.9}_{-19.6}$	24.9	0.18
20.7	16	$109^{+10.8}_{-11.6}$	43.7	0.16
21.2	16	$154^{+21.9}_{-21.0}$	76.7	0.13
21.7	16	$245^{+34.7}_{-43.0}$	135	0.11
22.2	16	$383^{+48.2}_{-47.2}$	236	0.09
22.7	16	586^{+152}_{-180}	414	0.07
23.2	16	879^{+130}_{-117}	726	0.06
23.7	16	1572^{+373}_{-454}	1273	0.05
24.2	15	2498^{+393}_{-902}	2089	0.04

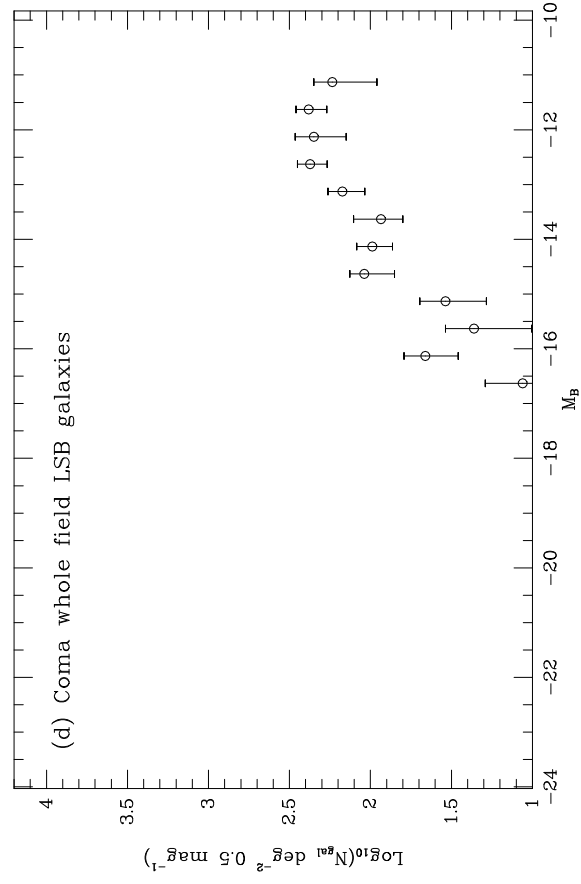
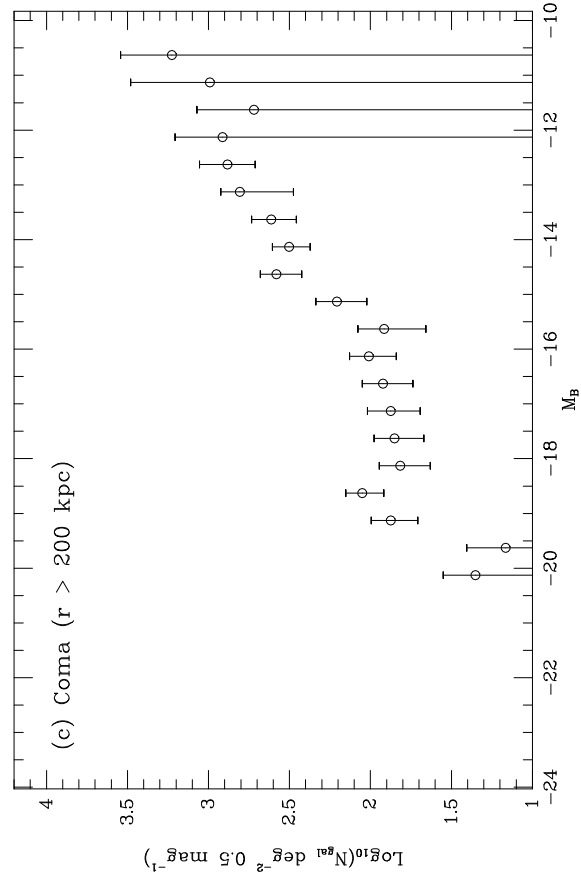
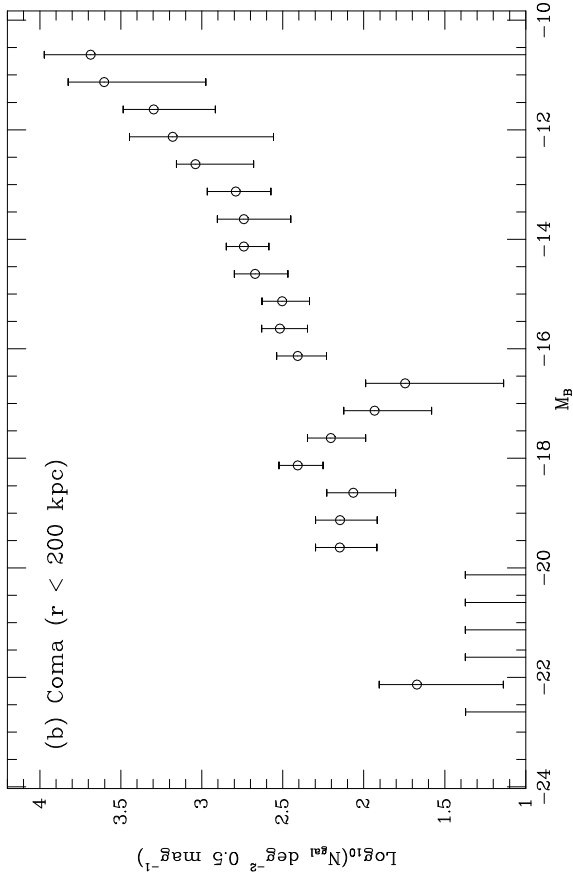
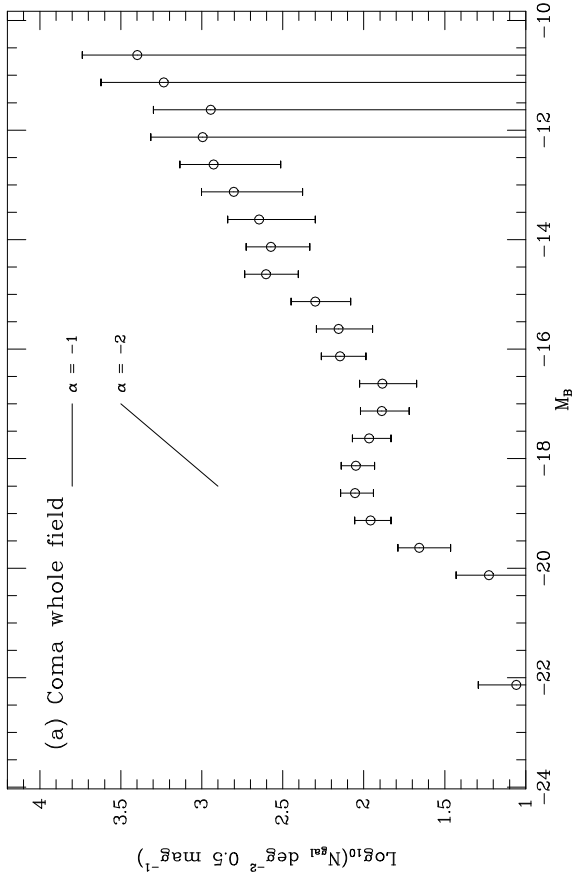


Table 5

Coma R band luminosity function

M_R	Number of Fields	$\log_{10} N$ (gal deg $^{-2}$ 0.5 mag $^{-1}$)	α_{12}	α_{13}	α_{33}	α_{34}
-21.61	16	$0.988^{+0.268}_{-0.834}$	—	—	—	—
-21.11	16	$1.825^{+0.115}_{-0.156}$	—	—	—	—
-20.61	16	$1.814^{+0.118}_{-0.161}$	-2.0	—	—	—
-20.11	16	$2.014^{+0.096}_{-0.123}$	-1.1	-1.5	-0.8	—
-19.61	16	$1.915^{+0.110}_{-0.148}$	-1.0	-0.9	-1.0	-0.6
-19.11	16	$1.884^{+0.119}_{-0.165}$	-0.7	-0.9	-0.6	-0.6
-18.61	16	$1.866^{+0.130}_{-0.186}$	-0.8	-1.0	-0.6	-0.8
-18.11	16	$1.732^{+0.172}_{-0.290}$	-1.2	-1.1	-1.1	-1.0
-17.61	16	$1.748^{+0.191}_{-0.348}$	-1.4	-1.4	-1.4	-1.5
-17.11	16	$2.107^{+0.125}_{-0.242}$	-1.9	-1.6	-2.1	-1.9
-16.61	16	$2.052^{+0.186}_{-0.247}$	-1.9	-1.7	-2.0	-1.8
-16.11	16	$2.455^{+0.096}_{-0.180}$	-1.6	-1.8	-1.5	-1.7
-15.61	16	$2.450^{+0.130}_{-0.143}$	-1.8	-1.8	-1.7	-1.8
-15.11	16	$2.470^{+0.143}_{-0.371}$	-1.7	-1.6	-1.9	-1.9
-14.61	16	$2.828^{+0.160}_{-0.181}$	-1.5	-1.2	-1.9	-1.1
-14.11	16	$2.992^{+0.065}_{-0.103}$	-0.9	-1.3	-0.6	-1.1
-13.61	16	$2.653^{+0.173}_{-0.560}$	-0.9	-1.2	-0.5	-0.7
-13.11	16	$2.469^{+0.317}_{-0.754}$	-1.0	-1.4	-0.8	-1.7
-12.61	16	$3.017^{+0.247}_{-0.411}$	-2.2	-0.9	-3.1	—
-12.11	16	$2.823^{+0.642}_{-\infty}$	-0.9	—	—	—
-11.61	15	$3.646^{+0.131}_{-0.387}$	—	—	—	—
-11.11	6	$2.014^{+1.466}_{-\infty}$	—	—	—	—

Table 6

Coma B band luminosity function

M_B	Number of Fields	$\log_{10} N$ (gal deg $^{-2}$ 0.5 mag $^{-1}$)	α_{12}	α_{13}	α_{33}	α_{34}
-20.13	16	$1.228^{+0.201}_{-0.386}$	—	—	—	—
-19.63	16	$1.657^{+0.133}_{-0.192}$	—	—	—	—
-19.13	16	$1.959^{+0.098}_{-0.127}$	-2.0	—	—	—
-18.63	16	$2.054^{+0.089}_{-0.113}$	-1.4	-1.5	-1.2	—
-18.13	16	$2.049^{+0.091}_{-0.115}$	-0.9	-1.1	-0.7	-0.7
-17.63	16	$1.967^{+0.103}_{-0.135}$	-0.8	-1.0	-0.5	-0.7
-17.13	16	$1.889^{+0.132}_{-0.169}$	-1.1	-1.1	-1.0	-1.0
-16.63	16	$1.885^{+0.142}_{-0.212}$	-1.3	-1.2	-1.4	-1.2
-16.13	16	$2.145^{+0.116}_{-0.159}$	-1.5	-1.5	-1.6	-1.7
-15.63	16	$2.155^{+0.138}_{-0.210}$	-1.8	-1.7	-1.8	-1.8
-15.13	16	$2.300^{+0.148}_{-0.219}$	-1.7	-1.6	-1.8	-1.7
-14.63	16	$2.604^{+0.131}_{-0.200}$	-1.6	-1.6	-1.7	-1.6
-14.13	16	$2.574^{+0.152}_{-0.239}$	-1.5	-1.6	-1.4	-1.6
-13.63	16	$2.647^{+0.192}_{-0.348}$	-1.4	-1.5	-1.4	-1.5
-13.13	16	$2.802^{+0.199}_{-0.425}$	-1.6	-1.4	-1.7	-1.4
-12.63	16	$2.926^{+0.209}_{-0.413}$	-1.4	-1.5	-1.3	-1.5
-12.13	16	$2.995^{+0.320}_{-\infty}$	-1.4	-1.6	-1.3	—
-11.63	16	$2.944^{+0.354}_{-\infty}$	-1.6	—	—	—
-11.13	16	$3.235^{+0.387}_{-\infty}$	—	—	—	—
-10.63	15	$3.399^{+0.338}_{-\infty}$	—	—	—	—

Table 7**Comparison of Coma Cluster photometric surveys**

Survey	Filter*	Area deg ²	Limiting Mag.	Sample size**
This work	<i>R,B</i>	0.18	$R = 23.5$	~ 1650
SH96	<i>R,B</i>	0.19	$R = 22.5$ (80%)	~ 800
Lobo et al. (1996): L96	<i>V</i>	0.40	$V = 21$	1025
Bernstein et al. (1995): B95	<i>R</i>	0.015	$R = 23^\dagger$	83
Thompson & Gregory (1993) ^{††} : TG93	<i>b</i>	3.97	$b = 20$	~ 1000
Godwin & Peach (1977): GP77	<i>V</i>	1.49	$V = 17.5$	~ 500

*The filter systems here are described in the original papers. Approximate colours for the cluster galaxies are $b - V = 0.8$ (Thompson & Gregory 1983) and $V - R = 0.7$.

**The sample sizes represent the numbers of galaxies following background subtraction, where one was made.

[†]This is not the limiting magnitude of the B95 data. Rather, it is the magnitude above which the galaxy luminosity function cannot be determined because of globular cluster contamination. The limiting magnitude is $R = 26$, brighter than which there are 1480 objects (including globulars).

^{††}This dataset includes galaxies from Godwin et al. (1983).

